FLORE
Repository istituzionale dell'Università degli Studi di Firenze

An experimental investigation on mass failures occurring in a riverbank composed of sandy gravel

(Article begins on next page)

10 April 2024

ELSEVIER

An experimental investigation on mass failures occurring in a riverbank composed of sandy gravel

L. Nardi, M. Rinaldi *, L. Solari

Department of Civil and Environmental Engineering, University of Florence, Via S. Marta 3, Firenze 50139, Italy

ARTICLE INFO

ABSTRACT

This paper reports the results and interpretation of laboratory experiments carried out on a model of a relatively coarse (sandy gravel) riverbank, with the aim of investigating the basic processes and possible factors of instability. After a series of initial tests, three main experiments were carried out in a glass walled tank, where a bank model was built with bank angles varying from 75° to 90°, bank height of 70 cm, and same sediment mixture (60% gravel, 40% sand), but with the addition of 1% of cement in the third experiment only. During the experiments, the bank was subject to a given hydrograph associated with a static oscillation of the water level and corresponding variations in pore water pressures were measured. Results show the occurrence of a large variety of processes (including erosion and failures because of loss of matric suction, cantilever, slab and slide failures, and granular flows) during the ascending phase of the hydrograph. Bank instability was related to a superimposition of initial (geometric) factors, and progressive reduction of apparent cohesion during the rising water stage. Apparent cohesion was sufficient to maintain a stable bank in loose material, but only for low bank height and/or slopes, whereas a limited percentage of cement is able to explain a markedly different response in terms of stability and mechanisms of failure.

© 2011 Elsevier B.V. All rights reserved.

1. Introduction

Bank failure is a key process in meandering channels, and its quantification is a challenging issue for advances in interpretation and prediction of the altimetric and planimetric evolution of river meanders.

The majority of studies dealing with modelling bank failures are focused on fine-grained (sand, silt, and clay), cohesive banks. The retreat of these banks, often occurring along sandy rivers and tidal channels, has been mainly related to instability and mass wasting processes (e.g. Darby and Thorne, 1996; Rinaldi and Casagli, 1999; Simon et al., 2000; Rinaldi et al., 2004; Rinaldi and Darby, 2008), and has been assessed using algorithms originally developed in the geotechnical field.

Riverbanks, totally or partially composed of relatively coarse, granular sediment (gravel or cobble mixed with sand), are also common along meandering channels with relatively coarse bed material, or other transitional gravel-bed channel morphologies (e.g. sinuous with alternate bars or wandering) where bank retreat is a key process in meander initiation and development. These types of banks, however, have received less attention compared to fine-grained, cohesive banks. As a consequence, models of coarse-grained bank stability are limited, and a tendency exists to oversimplify the complex nature and response of such banks.

Along composite banks, the failures occurring within the upper, cohesive layer are strongly related to the processes occurring within the basal layer of coarse material (e.g. Rinaldi et al., 2008; Luppi et al., 2009). Field evidence suggests that the processes acting on coarse sediment at the bank toe are extremely variable with combinations of fluvial entrainment and a variety of small-scale mass failures. Mixtures of granular sediment (gravel, cobble) with a fine interstitial matrix (predominantly sand) often exhibit an intermediate response between loose and partially cohesive sediment.

Morphodynamic models of the evolution river planforms traditionally consider fluvial entrainment and erosion as the most important, if not the exclusive, mechanism for bank retreat. In many models bank retreat is evaluated through over-simplified schematizations based, for instance, on the knowledge of the near bank flow velocity and some erodibility coefficient (e.g. Ikeda et al., 1981; Lancaster and Bras, 2002; Seminara, 2006; Frascati and Lanzoni, 2009).

Increasing efforts have been recently made to include the erosion of granular layers at the bank toe in morphodynamic and regime models, but the most common geotechnical model for coarse material is that of infinite slope failure, that corresponds to the assumption of an ultimate stable angle equal to the angle of repose (see for instance Nagata et al., 2000; Eaton et al., 2004; Eaton, 2006; Chen and Duan, 2006, 2008; Dulal et al., 2009). This model is able to reproduce the geometry of the wedge of loose sediment often accumulated at the bank toe, but it is not suitable for explaining near-vertical faces of coarse sediment, with angles much higher than the angle of repose, that are often observed in nature. To explain such geometries, different models and additional factors need to

be considered, including effects of apparent cohesion acting in the matrix of fine sediment, packing, partial cementation of the material, and vegetation.

This research aims to investigate the basic processes controlling the stability of relatively coarse, granular bank sediments, by carrying out a series of laboratory physical experiments.

Physical experiments have been rarely adopted in the past for riverbank processes, given difficulties in scale reproduction, with particular reference to scaling sediment sizes. Only more recently has an increasing employment of laboratory experiments occurred, including investigations of bank failures. For example, various works have been carried out to investigate dam-break flow and associated downstream sand bank failures (Spinewine et al., 2002; Soares-Frazao et al., 2007; Spinewine and Zech, 2007; Zech et al., 2008). Other works have carried out experiments on small scale banks composed of fine-grained, sandy sediments, with specific focus on the occurrence of seepage erosion processes because of seepage flow gradients and related mass failures (Howard and McLane, 1988; Fox et al., 2006, 2007; Wilson et al., 2007; Lindow et al., 2009).

In this research, we started from an experimental setup similar to that used in these latter works, but with the intent to extend the observations to coarser sediment and associated basic processes. The Cecina River (Tuscany, Central Italy) has been used as a reference study case, and the bank reconstructed in the laboratory was intended to mimic a coarse-grained layer of the basal portion of a typical bank profile of this river. The experimental setup and some preliminary results have already been reported in Nardi et al. (2009). In this paper, however, the results of all the experiments carried out, and their analysis and interpretation are reported. The experimental activity was focussed on processes related to gravity (mass failures) and to the interaction between water and sediment, whereas flow entrainment was not modelled for technical limitations of the experimental setup. Whereas this was obviously a limitation, it allowed for the exploration of how the stability of a coarse bank is affected by processes associated to bank geometry and changing pore water pressures, independently of flow only.

The specific objectives of this paper can be summarised as follows: (1) investigate the dominant processes acting on banks composed of loose or slightly cemented sediment; (2) identify the different mechanisms of failure in the reproduced banks; (3) understand initiation of the investigated processes and factors controlling stability, in particular, the role of apparent cohesion and cementation in maintaining bank stability; and (4) investigate the importance of initial instability conditions related to bank geometry or transient changes in bank stability because of the action of water. The overall findings may be instrumental to the development of more realistic algorithms of coarse-grained bank retreat for incorporation into hydro-morphodynamic models of river planimetric and bed evolution.

2. Experimental setup and data collection

The characteristics of the bank model were defined based on a series of observations and grain-size analyses carried out on basal layers of composite riverbanks along the Cecina River (Tuscany, Central Italy) (Fig. 1). The selection of the Cecina River as a reference field study case is motivated by various reasons, including: (1) the presence of actively eroding composite banks (Fig. 1B), consisting of a basal layer of packed and slightly cemented gravel, with generally a wedge of loose gravel and cobble located at the bank toe, and an upper fine-grained (predominantly sandy silt) cohesive portion of the bank; (2) existing research activities on riverbank processes along this river (see Rinaldi et al., 2008; Luppi et al., 2009). The bank reconstructed in the laboratory was not intended to scale an entire bank profile of the Cecina River, but rather to mimic a single layer of the basal portion, to investigate the basic processes occurring on this part of the bank. The grain-size distribution of the basal gravel layer along Cecina riverbanks is quite variable, and we

selected as reference the grain-size distribution of layers composed of finer gravel and sand.

We started with a series of experiments carried out in small boxes to test the responses, in terms of processes and stability, of different sediment mixtures, hydrographs, and bank geometries (Fig. 2). For example, in this phase we tested which possible sediment mixture (relative percentage of sand) appeared to be more suitable to reproduce the desired mass failures, avoiding excessive stability or instability. The boxes were constructed of wood, with a rectangular base of 45 × 50 cm and a height of 40 cm, and a frontal wooden panel with an assigned slope angle which was removed at the start of the test. During the tests, the boxes were placed in the tank, and subject to given hydrographs, with a peak water stage of 25 cm, and a total duration of 1 h and 40 min. A summary of the initial tests carried out is reported in Table 1. The results of these tests were used in the later analyses for classification of different failure mechanisms and observations on instability conditions, as some mechanisms were more frequently observed in these tests than during the main experiments.

For the main experiments, a tank was specifically designed and built (Fig. 3A). The tank is 1 m wide, 3 m long, and 1 m high, having a steel structure, a zinc platted bottom, and glass walls to allow for observations and video monitoring during the experiments. The front side is constructed of a zinc platted door to allow for the construction of the bank inside the tank. A smaller reservoir is included on the back of the tank to maintain a given water head during the experiments, with a porous plate separating the reservoir from the main body of the tank ("lysimeter" modality, according to the experimental setup developed by Fox et al., 2006).

This experimental layout was designed to reproduce the effects of: (1) movement of water from the river into the bank and vice versa, and consequent changes in pore water pressures; (2) lateral confining water pressures; and (3) possible seepage induced erosion by groundwater gradients towards the river, in case of imposing a water head higher than the river stage in the reservoir back of the bank (this option was not used in the experiments described here). The effect of fluvial entrainment from the boundary shear stresses along the bank is not reproduced.

A bank model was then built inside the tank. As already pointed out, the bank model was intended to mimic the geometry and grain-size distribution commonly found in the basal layer of the riverbanks along the Cecina River. Based on field observations, a bank height of 70 cm was selected, while slope angles varied from 75° to 90°.

For the first experiment (EXP1), the bank was 1 m wide, with a base of about 133 cm in length, and a slope angle of 75°. The sediment mixture was composed of about 60% gravel ($D_{50} = 5.9$ mm), and 40% sand ($D_{50} = 0.3$ mm) (the amount of silt and clay was negligible). The sediment mixture was initially wetted, with an initial water content of about 6–7% (see also the Experimental results). Saturated hydraulic conductivity was estimated to be $k_{sat} = 3.64 \times 10^{-6}$ m s^{-1} by laboratory tests.

In the following two experiments (EXP2 and EXP3), the size of the bank was about the same, but the slope angle was set at 90°. The sediment mixture was also the same, but for EXP3 a small quantity of cement (1%) was added. Experimental research on naturally cemented sediment is rare because of extreme difficulties in acquiring undisturbed samples (Haeri et al., 2005). Because recreating natural conditions of cementation is not possible in the laboratory, we used an artificially cemented mixture to simulate the different responses (related to the increased shear strength) because of possible precipitation of various agents (salts) from circulating interstitial water in natural riverbanks.

A summary of the geometries and sediment mixtures used for the three experiments is reported in Table 1.

The compaction of sediments was obtained by applying a static load that varies from 0.045 to 0.013 kg/cm^2; these values are somewhat similar to the lithostatic loads acting on the basal layer by the presence of an upper cohesive layer. The bank was built by creating a series of
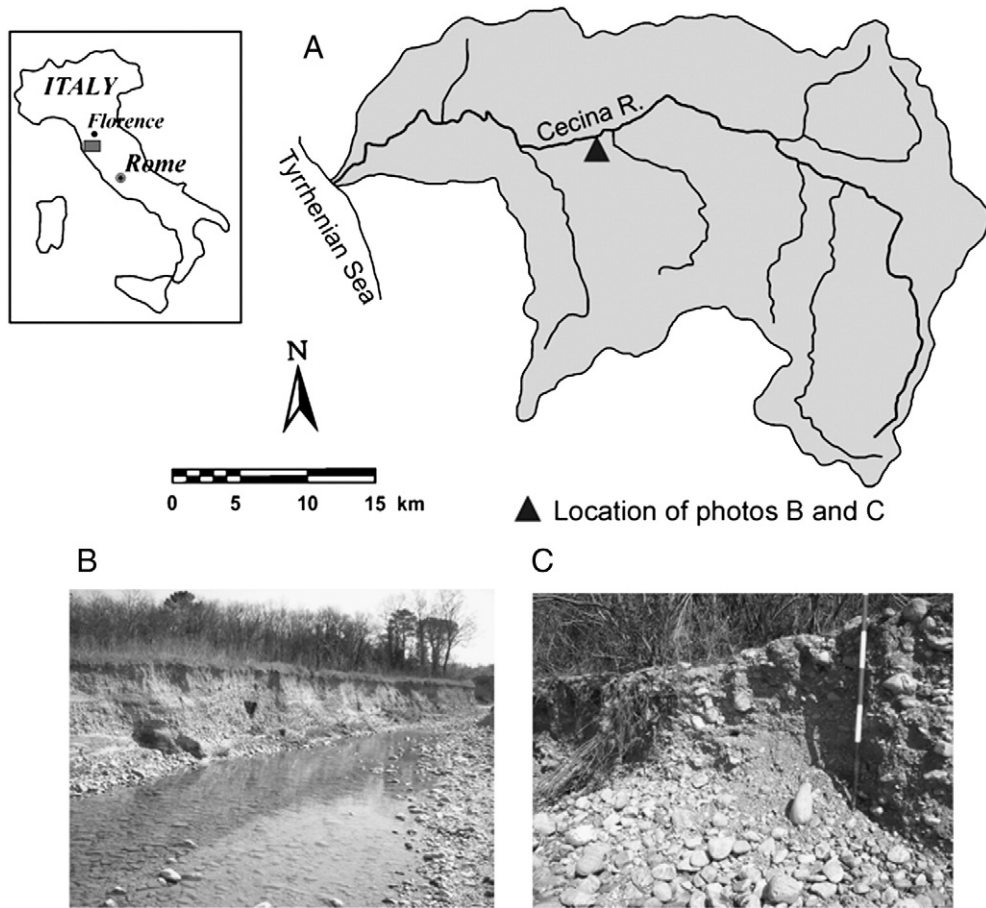
Fig. 1. Location of the Cecina River. A: Cecina basin; B: eroding composite riverbank of the Cecina River; C: detail of a coarse-grained bank with evidence of mass failure.

10 cm layers, until a given bank height was obtained. A distributed load (made by steel plates: see Fig. 3B) was applied to the top of each layer, with a weight decreasing from the bottom to the top of the bank model. Each layer was left under the assigned load for about 20 h to allow for a sufficient consolidation. Measurements of changes in the thickness of each layer before and after consolidation were carried out. We also considered the option of a dynamic compaction by using a mechanical earth compactor, but this was excluded for the following reasons: (1) to avoid damages to the tank; (2) to avoid the formation of interstitial over-pressures; and (3) because static compaction better reproduce the conditions that normally occur in nature from lithostatic loads.

The unit weight of sediments was estimated to be 14.4 kN/m^3 in the initial conditions (loose sediment), increasing up to about 15.2 kN/m^3 after compaction.

During construction of the bank and compaction, a wooden panel was positioned to assign a given slope angle to the bank (see Fig. 3B). The panel was removed immediately before the start of each experiment. For EXP1, a basal failure occurred immediately after the panel removal (see Section 3 for details). This unforeseen collapse could be in part explained by limited compaction of the material along the slope boundary, as in that portion of the bank the application of the load was more difficult, and the portion of sediment directly in
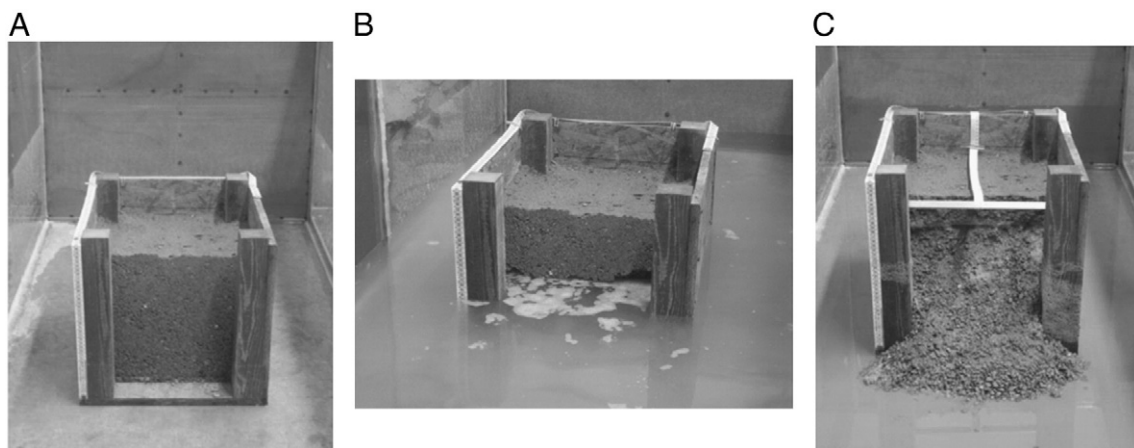
Fig. 2. Initial tests. A: Beginning of test 4; B: rising phase of test 4; C: conclusion of test 4.

Table 1
Summary of bank geometries and sediment mixtures used during the initial tests (in small boxes) and the main experiments (in the tank). *H*: bank height; β: bank slope; G: gravel; S: sand; C: cement.

	Bank geometry	Sediment mixture
Initial tests		
Test 1	$H = 22$ cm, $\beta = 70°$	75% G–25% S
Test 2	$H = 22$ cm, $\beta = 70°$	60% G–40% S
Tests 3, 5	$H = 30$ cm, $\beta = 75°$	75% G–25% S
Test 4	$H = 30$ cm, $\beta = 75°$	54% G–37% S–9% Silt
Test 6	$H = 30$ cm, $\beta = 75°$	60% G–40% S
Tests 7, 8	$H = 30$ cm, $\beta = 75°$	60% G–40% S
Tests 9, 10, 11, 12	$H = 30$ cm, $\beta = 90°$	60% G–40% S
Test 13	$H = 30$ cm, $\beta = 90°$	60% G–39.5% S–0.5% C
Tests 14, 15, 16	$H = 30$ cm, $\beta = 90°$	59.5% G–39.5% S–1% C
Tests 17, 18, 19	$H = 30$ cm, $\beta = 90°$	59% G–39.5% S–1.5% C
Main experiments		
EXP1	$H = 70$ cm, $\beta = 75°$	60% G–40% S
EXP2	$H = 70$ cm, $\beta = 90°$	60% G–40% S
EXP3	$H = 70$ cm, $\beta = 90°$	59.5% G–39.5% S–1% C

contact with the panel was not really subject to vertical overloads. Consequently, the assigned bank slope angle was changed to 90° for EXP2 and EXP3 (Fig. 3C). A failure, however, also occurred at the beginning of EXP2, which did not occur in EXP3, presumably because of the presence of cement in the sediment mixture (reasons for the occurrence of an initial failure for EXP1 and EXP2 are discussed later).

To measure pore pressure, a series of five tensiometers and one TDR (Time Domain Reflectometry) were installed inside the bank, in a vertical position at different distances from the bottom. In particular, three tensiometers were positioned along one lateral side of the bank, and the other two along the rear side; the TDR was placed in the rear corner near the tensiometers (Fig. 3D). Based on the results of the first experiment, the configuration was optimised by some small changes in the position of the tensiometers. For example, tensiometer T1 was located further away from the bank slope to avoid disturbance to initial failures. Planimetric and vertical positions of each of the tensiometers and TDR during the three experiments are listed in Table 2. Because of the coarse sizes of the sediments, the instruments were installed during the construction of the bank, by inserting them
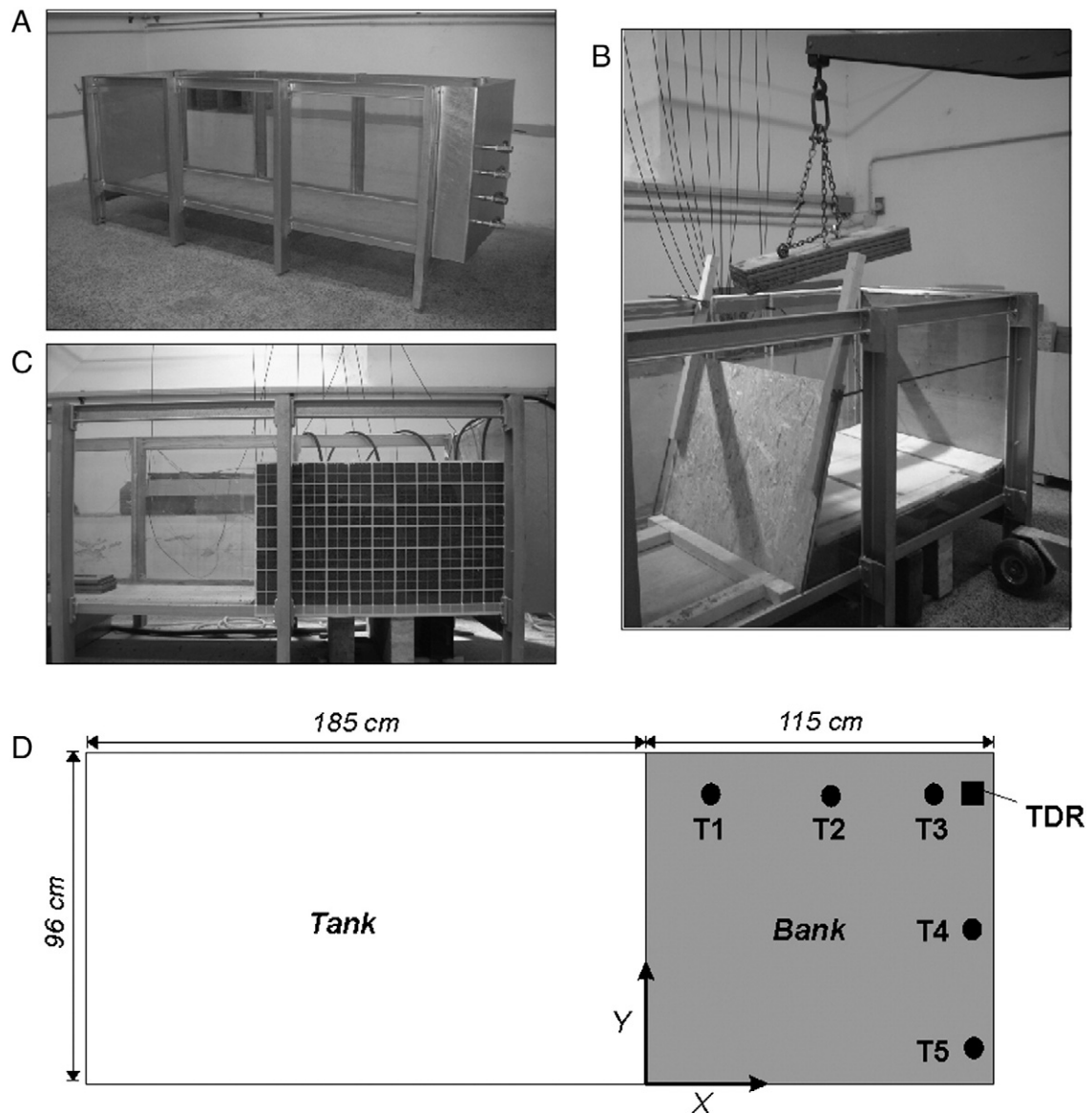
Fig. 3. Experimental setup. A: tank; B: loads made by steel plates and setup of the wooden panel during the construction of the bank physical model; C: bank model for EXP3; D: configuration of monitoring instruments (for positions and depths of each of the instruments see Table 2).

Table 2

Planimetric and vertical positions of tensiometers and TDR during the three main experiments. X and Y: planimetric coordinates (see Fig. 3); Z: elevation above the bottom of the bank.

	EXP1			EXP2			EXP3		
	X (cm)	Y (cm)	Z (cm)	X (cm)	Y (cm)	Z (cm)	X (cm)	Y (cm)	Z (cm)
T1	21.5	89.3	37	35.5	89.3	27	35.5	89.3	27
T2	61.5	89.3	37	71	89.3	39	71	89.3	39
T3	96	89.3	37	101	89.3	52	101	89.3	52
T4	112	48	54	110	48	39	110	48	39
T5	112	6	64	110	6	27	110	6	27
TDR	112	89.3	30	110	89.3	45	110	89.3	45

in steel pipes placed vertically into the sediment, and then removing the pipe after the material had completely covered the length of the sensors. The water stage was measured by an ultrasonic distance sensor with an accuracy of ±2 mm. All of the sensors were connected to a data logger set to acquire and record data every 30 s.

Imposed boundary conditions for the three experiments include the hydrograph and the water stage in the lysimeter in the back of the bank. A hydrograph was imposed, with similar characteristics for the three

experiments (Fig. 4), and with a shape similar to that observed in a series of monitored flow events occurred on the Cecina River (see Luppi et al., 2009).

During EXP1, a peak of 59.89 cm was reached in 3 h and 14 min, whereas the descending part of the hydrograph was slightly longer, for a total duration of 6 h and 40 min. The water stage in the lysimeter was maintained constant once the water exceeded 34 cm from the bottom of the bank by opening the lowest valve located behind the lysimeter. This
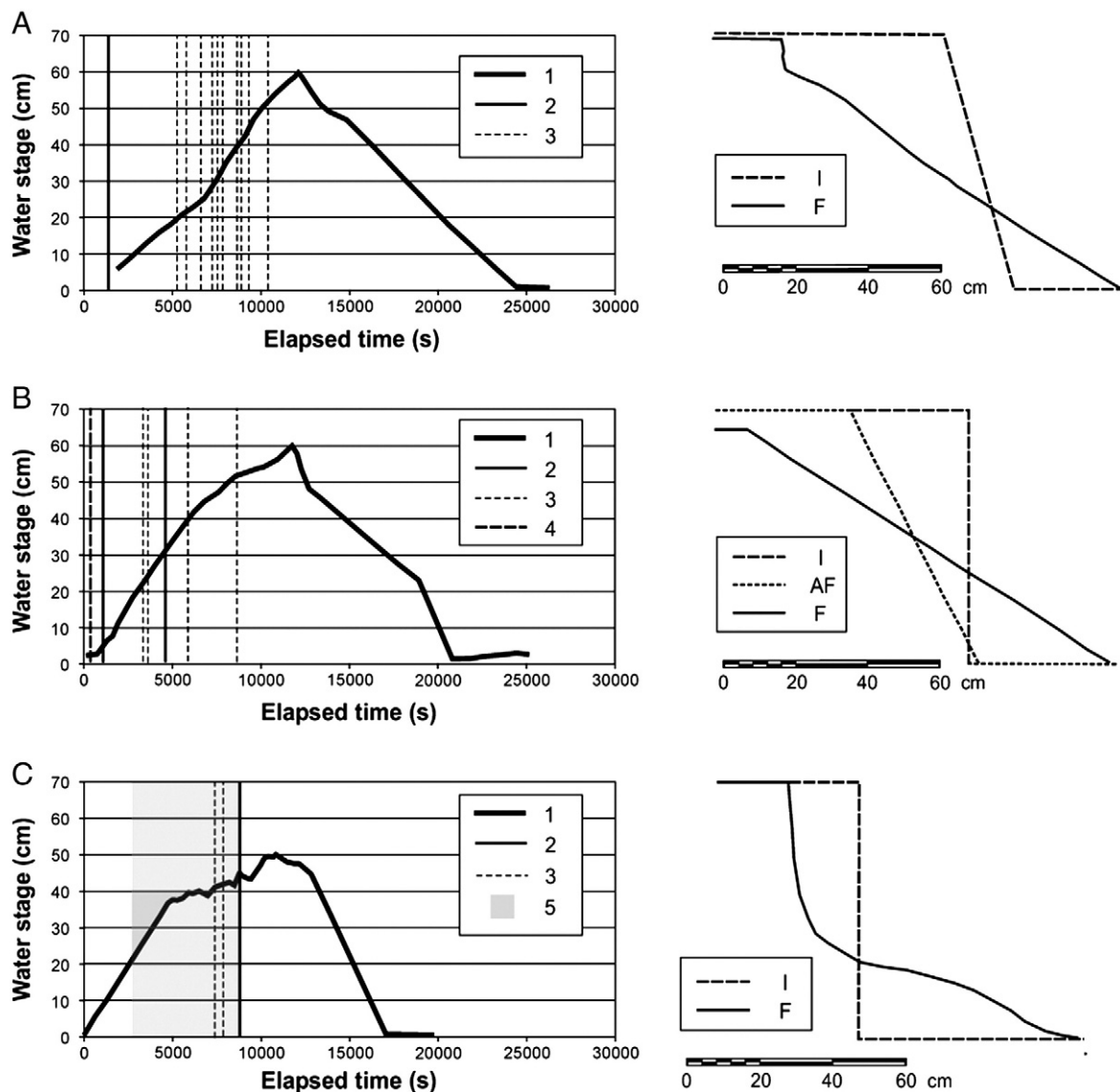
Fig. 4. Summary of hydrographs, failures and profile evolution during EXP1 (A), EXP2 (B), and EXP3 (C): hydrograph and failures (on the left), and changes in bank profile (on the right). 1: Hydrograph; 2: large failures; 3: small failures; 4: initial failure immediately after the panel removal; 5: progressive erosion because of loss of matric suction; I: initial profile; F: final profile; AF (in EXP2): new profile after immediate failure.

layout was set to simulate a water outflow discharge through the side on the back of the tank, thus avoiding an excessive and unrealistic accumulation of water within the volume of the bank model.

During EXP2, a peak of 59.6 cm was reached in 3 h and 6 min and the total duration of the test was 6 h. The water stage in the lysimeter was kept constant at 34 cm.

A lower peak of the hydrograph was reached during EXP3. As in the previous experiments, the water stage at the lysimeter was maintained at 34 cm. Because of an excessive outflow discharge from the valve at the back, which was not balanced by the inflow discharge in the tank in the third experiment, it was not possible to obtain water stages higher than 50.3 cm. This stage was reached in 2 h and 59 min. The greater outflow discharge probably resulted from a higher conductivity of the sediment with cement (see also Section 3.4). The total duration of this experiment was about 5 h.

During the experiments, a video and periodic photos were acquired from frontal and lateral positions. Furthermore, some additional measurements were carried out, including: (1) water stage in the lysimeter; (2) water discharge outflowing the valve; and (3) bank profiles which were drawn on transparent sheets placed on one lateral glass of the tank for every mass failure to provide time lines of the bank evolution. Videos recorded from frontal and lateral positions allowed one to verify when bank changes occurred locally on the lateral side or on the entire bank. Since the water was clear during the drawdown phase, no measurements of turbidity was collected.

3. Experimental results

All the data collected during each experiment were processed and analysed through the following steps: (1) systematic identification and classification of all mass failures; and (2) temporal trends of measured hydrological parameters (water stage, pore water pressures, water content), and the relations with observed processes. Accordingly, this section is organised in four parts: (i) a classification and description of the different mechanisms of failure observed in all the experiments (including the initial tests in the small boxes); (ii) some observations from the initial tests; (iii) the succession of processes observed for each of the main experiments; and (iv) trends of measured hydrological parameters during the main experiments.

3.1. Types of observed mass failures

For the description of the results, it is useful to define and classify the observed mechanisms of failure that occurred during the three main experiments and the initial tests.

1) Erosion and failures because of loss of matric suction. This process is related to a loosening of the weak links between particles as soon as the pores are saturated by water and the resulting increased weight of aggregates or small blocks from sediment saturation (see also the discussion). The erosion process initially produces a scour at the bank toe (Fig. 5, case A1), followed by small-scale mass failures, resulting in the collapse of the upper small block or aggregate of particles by tensile failure (Fig. 5, case A2).
2) Cantilever failures. These are the most frequently observed failures, and are often the consequence and evolution of the previous mechanism, or of basal slide (alcove-shaped) failures (see mechanism 4). All the three types of cantilever failures have been observed: shear, tensile, and beam failures (following Thorne and Tovey, 1981). Shear failures are defined here as failures occurring by shear along a vertical and lateral surface delimiting the cantilever block up to the bank top (Fig. 5, case B1). Tensile failure is defined as a failure along a horizontal upper surface of the failing block in which the detachment occurs by tensile stress (Fig. 5, case B2). In some cases, a beam cantilever failure was also observed (Fig. 5, case B3), with a rotational component (toppling) of the movement.

3) Slab failures. They are classified separate from the cantilever beam failures because they do not occur on cantilevered, undercut blocks, but usually involve relatively small blocks on the bank top detached by deep tension cracks which stand on the top of the debris cone derived from previously failed material (Fig. 5, case C).
4) Slides. This type of failure, very common along cohesive river-banks, was observed only on a few occasions during the experiments. We distinguish two modes of slide failures: (1) small-scale slides on the middle and lower portion of the bank with a slight rotational component (Fig. 5, case D1); (2) rotational failure involving the whole bank, with a slightly concave slip surface emerging on the bank top (or eventually with a short tension crack) (Fig. 5, case D2). The first type can be actually described as a combination of detachment of material under tensile stress along an arcuate surface and a contemporary slide, resulting in an alcove-shaped surface, similar to what has been frequently observed along steep fine-grained banks (Bradford and Piest, 1977, 1980; Thorne et al., 1981; Dapporto et al., 2001, 2003). Although the resulting geometry can be sometimes similar to the failures because of loss of matric suction, it differs from it because it involves larger scale mass movement (rather than a "particle-by-particle" erosion). The second type was actually observed only on one occasion, and can be better described as a combination of slide and flow (see next mechanism).
5) Dry granular flow. It consists of an avalanche of granular, loose sediment, creating a fan-shaped debris accumulation close to the angle of repose (Thorne et al., 1996) (Fig. 5, case E). This was observed in one case as an initial mechanism of failure (EXP2), and in other cases as movement along the existing debris accumulation of failing material originated by other mechanisms.

## 3.2. Observations during the initial tests

As mentioned previously, quantitative measurements were not performed during the initial tests, but a series of qualitative observations were carried out. These included the following aspects: (i) instability of the bank and mechanisms of failure; (2) phase of the hydrograph (rising, peak, descending phase) at the time of the main failures. During a first group of tests (from 1 to 12), a range of sediment mixtures was tested varying the percentage of gravel and sand (Table 1). During these tests, the most common succession of processes included a first phase of erosion because of loss of matric suction, with creation of a basal scour, development of tension cracks and a subsequent series of cantilever failures, initially tensile and then shear (i.e. tests 4 and 5) or beam failures (i.e. tests 6 and 8). Erosion because of loss of matric suction occurred during the rising phase of the hydrograph, with a scour forming up to about the same level of the water stage. Observation of this process was possible during the tests because the initial bank face remained stable after the panel removal, so that water entered directly in contact with an intact, near-vertical bank. A similar evolution was observed only during EXP3 of the main experiments (as explained below). Besides erosion because of loss of matric suction, all the failures occurred during the rising phase of the hydrograph.

A second group of tests (from 13 to 19) included a small percentage of cement (Table 1). Some failures were observed during the rising phase of test 13 (0.5% of cement). No failures or tension cracks were observed with a higher percentage of cement (tests 14–19): only the detachment of small blocks at the bank toe, classified as failures because of the loss of matric suction, was noted during high water stages.

3.3. Occurrence of failures during the main experiments

Regarding the main experiments, the occurrence of mass failures at the scale of each hydrograph, and resulting modifications from the initial to the final bank profile, are reported in Fig. 4. In this figure, mass failures indicated as being large are those involving a significant
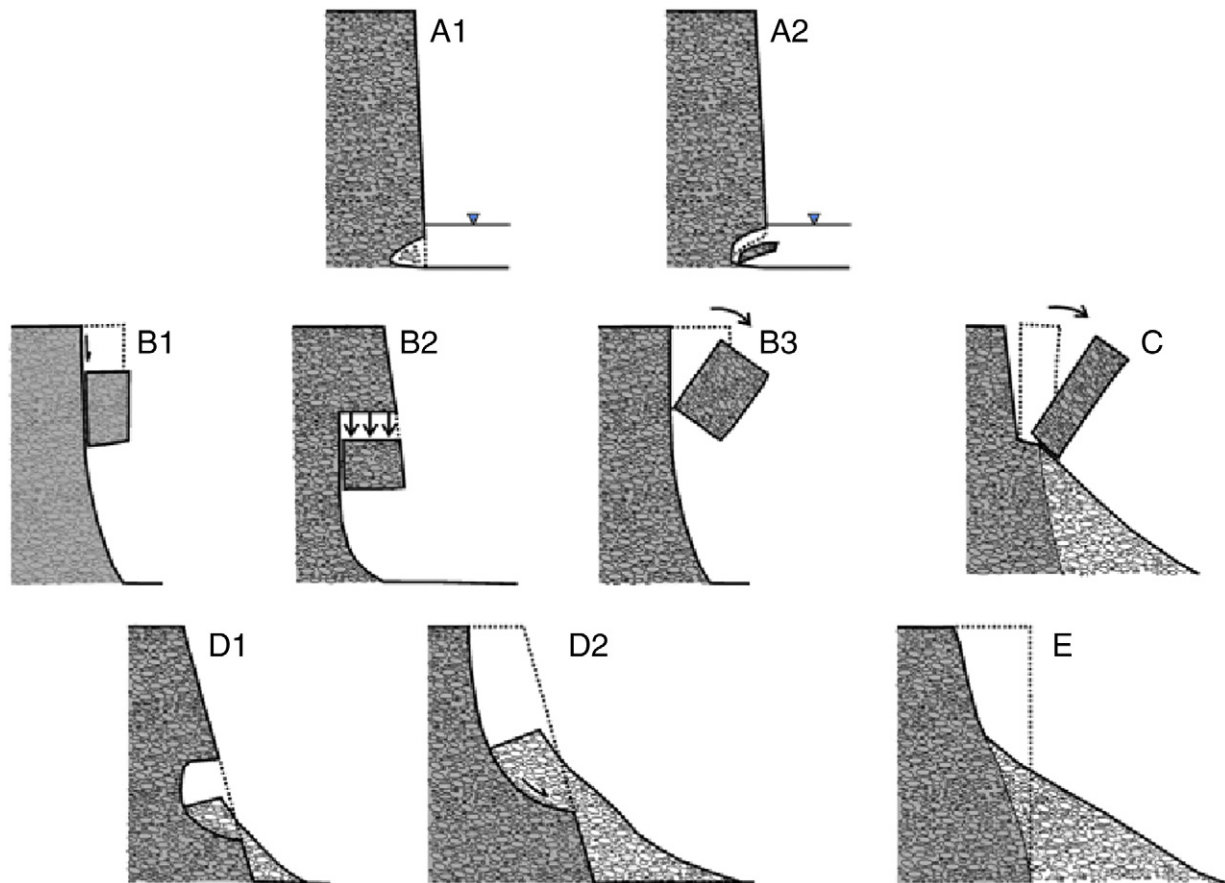
Fig. 5. Types of erosion processes. A: erosion (A1) and failure (A2) because of loss of matric suction; B: cantilever failures (B1: shear failure; B2: tensile failure; B3: beam failure); C: slab failure; D: slides (D1: alcove-type failure; D2: rotational slide); E: dry granular flow.

portion of the bank height and approximately the entire width, whereas small failures are those which occurred on localised portions of the bank profile and/or width. It is possible to observe that all the mass failures occurred during the rising phase of the hydrographs. In the case of the EXP1 and EXP2 the mass failures were distributed along the entire rising part of the hydrograph. In the case of EXP3, as effect of cementation and increased shear strength, the failures occurred exclusively in proximity of the peak of the hydrograph.

A summary of the evolution of bank profiles during each experiment is given as follows, with reference to the photos reported in Fig. 6.

EXP1. (1) A rotational (alcove-type) slide failure immediately occurred following the removal of the wooden panel. The failure covered the complete basal portion of the bank, up to about 30 cm from the toe. After about 10 min, a rapid succession of tensile and beam cantilever failures were observed, involving only the upper part of the right side of the bank. (2) After 18 min (elapsed time 28 min), a failure occurred involving the central portion of the bank, while a tension crack, created earlier, became progressively more evident. About 34 min later (elapsed time 62 min), a cantilever failure occurred on the left margin, followed by a failure in the middle part of the bank, and immediately after that (3) another cantilever on the left side. (4) About 62 min later (elapsed time 124 min), a large, arcuate failure surface appeared involving the entire width of the bank top, followed by (5) a succession of failures of blocks about 10 cm in width. Close to the peak of the simulated event, the profile reached the configuration of a nearly plane surface with a slope angle of about 35°. The bank maintained this geometry during the entire descending hydrograph, until (6) the end of the experiment.

EXP2. The initial bank slope was set at 90°, but immediately after the removal of the wooden panel, (1) a failure across the whole bank

occurred, classified as a granular flow in loose cohesionless material, creating a nearly plane surface. (2, 3) The failed material was removed from the bank toe, and the bank was shaped according to an angle of about 67° to continue the experiment. After 7 min and 20 s, a large rotational failure occurred involving the upper and middle portion of the whole bank. This can be better described as a flow slide, as multiple and temporary concave failure surfaces were observed. After this event, only other small failures occurred during the ascending phase of the hydrograph, until (4) the profile became a nearly planar surface with a slope of about 35°, corresponding approximately to the angle of repose for this sediment. Similarly to EXP1, the bank profile did not change during the descending phase of the hydrograph.

EXP3. The bank material in this last experiment included a small quantity of cement. Consequently, the bank showed a response different from previous experiments. (1) The initial bank was set at 90° and remained stable after the removal of the wooden panel. (2) After about 40 min, a scour because of loss of matric suction started to manifest along most of the basal area of the bank, but was more evident on the right and central part. This process started at the interface of different sub-layers of 10 cm built during the compaction procedure. The scour progressively continued to extend laterally and within the bank as time progressed. A first manifestation of failure involved a small block on the left margin located 10 cm below the water stage. This failure rapidly progressed upward as a tensile cantilever failure. (3) After 145 min and 54 s from the beginning, a rapid succession of further tensile failures occurred in various portions, until the cantilevered bank was completely up to the water stage. About 5 s later (elapsed time 146 min), a rapid succession of three cantilever failures occurred (the smaller was a tensile failure, the two larger were beam failures), recreating a nearly vertical bank face. (4) This became the final bank configuration, because
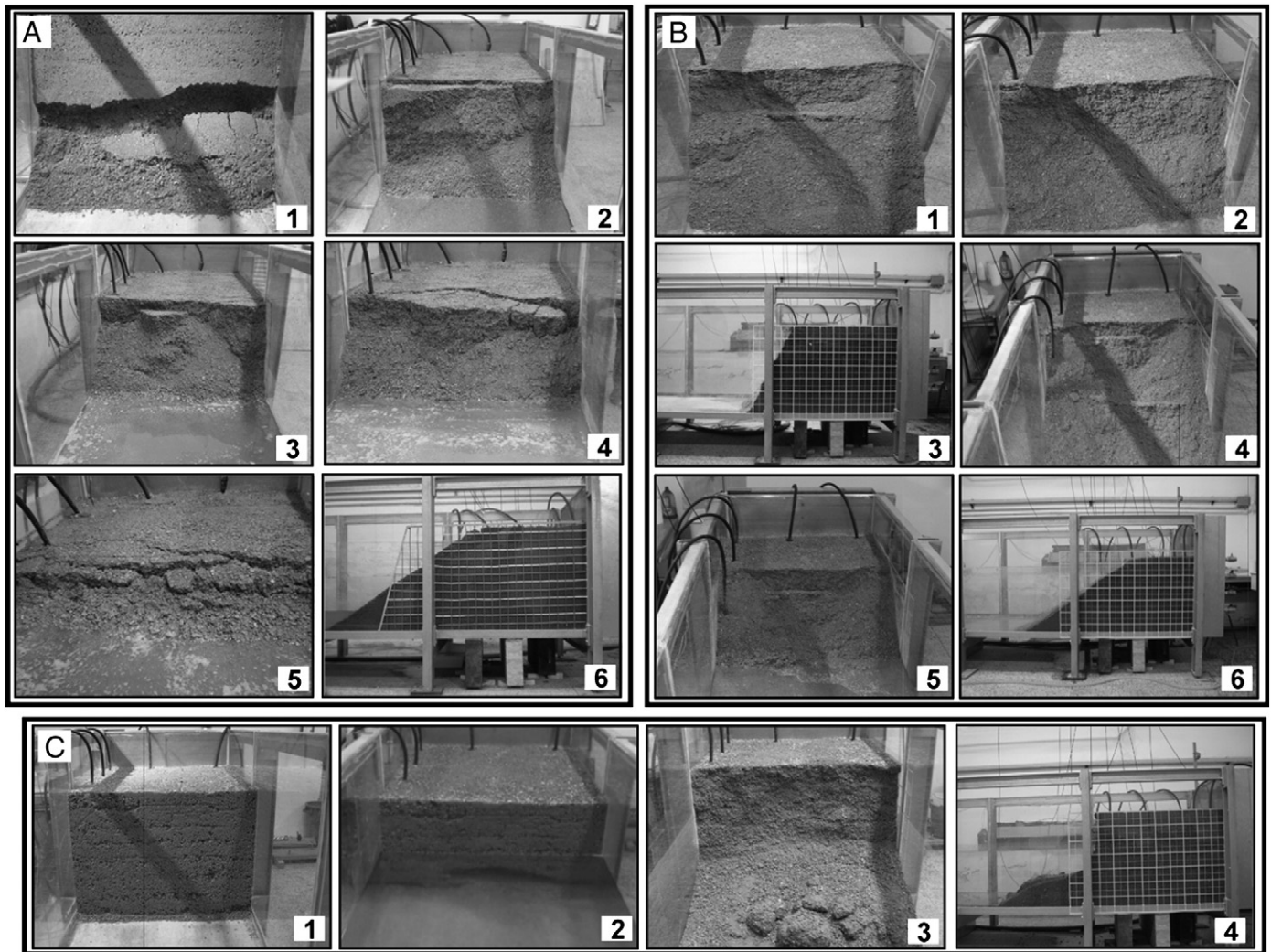
Fig. 6. Photos of bank profile evolution during some of the experiments. A: EXP1; B: EXP2; C: EXP3 (for the numbered photos see description in the text).

no failures occurred during the descending phase of the hydrograph, with a basal wedge of failed material at a slope angle of about 20° and some of the failed blocks still recognisable, and an approximately vertical face of about 40 cm.

3.4. Trends of hydrological parameters

Results, reported in Fig. 7, show the general trends of measured parameters and the occurrence of the failures during the three experiments, and are described as follows.

EXP1. In general, as it might be expected, pore water pressure increased with water stage and water content. Fig. 7A shows that, when the water stage was 37 cm, pore water pressure became positive at the tensiometers located at the same level (T1, T2 and T3), and the material surrounding the TDR was close to saturation, with the water content equal to 19.6%. This value in water content was constant also in the first part of the drawdown phase, until the water stage was 20 cm. The tensiometer T4 initially appeared not to respond to the imposed hydrograph, because values recorded were much lower than the others. This discrepancy became smaller, however, with the increase in water stage. The tensiometers at 37 cm, located in front of the bank and in the middle (T1 and T2), gave almost the same values, whereas T3 showed lower values during the first part of the test, to reach similar values to T1 and T2 after about 2 h from the

beginning of the experiment. It is possible that T3 and T4 were disturbed by localised phenomena such as drier material (water content not constant) or imperfect adherence between the material and the porous cup of the tensiometers.

Finally, tensiometer T5, located at the back of the bank at 64 cm from the bottom, did not reach the saturation, given that the peak of the hydrograph was lower (59.9 cm) than the elevation of the tensiometer.

EXP2. As mentioned before, for this experiment a slightly different configuration of the sensors was used (see Table 2): the trends of pore water pressures were, therefore, different from EXP1. Fig. 7B shows that T1 was the first tensiometer to reach saturation when the water stage was 32 cm, followed by T2 and T4, for water stages from 38 to 40 cm. T5 was located in a lower position than T4 and, at the beginning of the test, measured a pressure higher than T4. T5 reached saturation later, however, when the water stage was 43.5 cm. This happened because the reaction of T5 was slower than T4. T3 did not reach saturation because it was located in the back of the bank at 52 cm from the bottom, whereas the valve behind the lysimeter was open at 34 cm. TDR indicates that saturation at around 45 cm from the bottom of the bank, corresponding to the height of the sensor, occurred when the water stage was 51.4 cm. The water content of saturated material for this test was 20.9%.

During the descending phase of the hydrograph, the parameters decreased to similar final values.
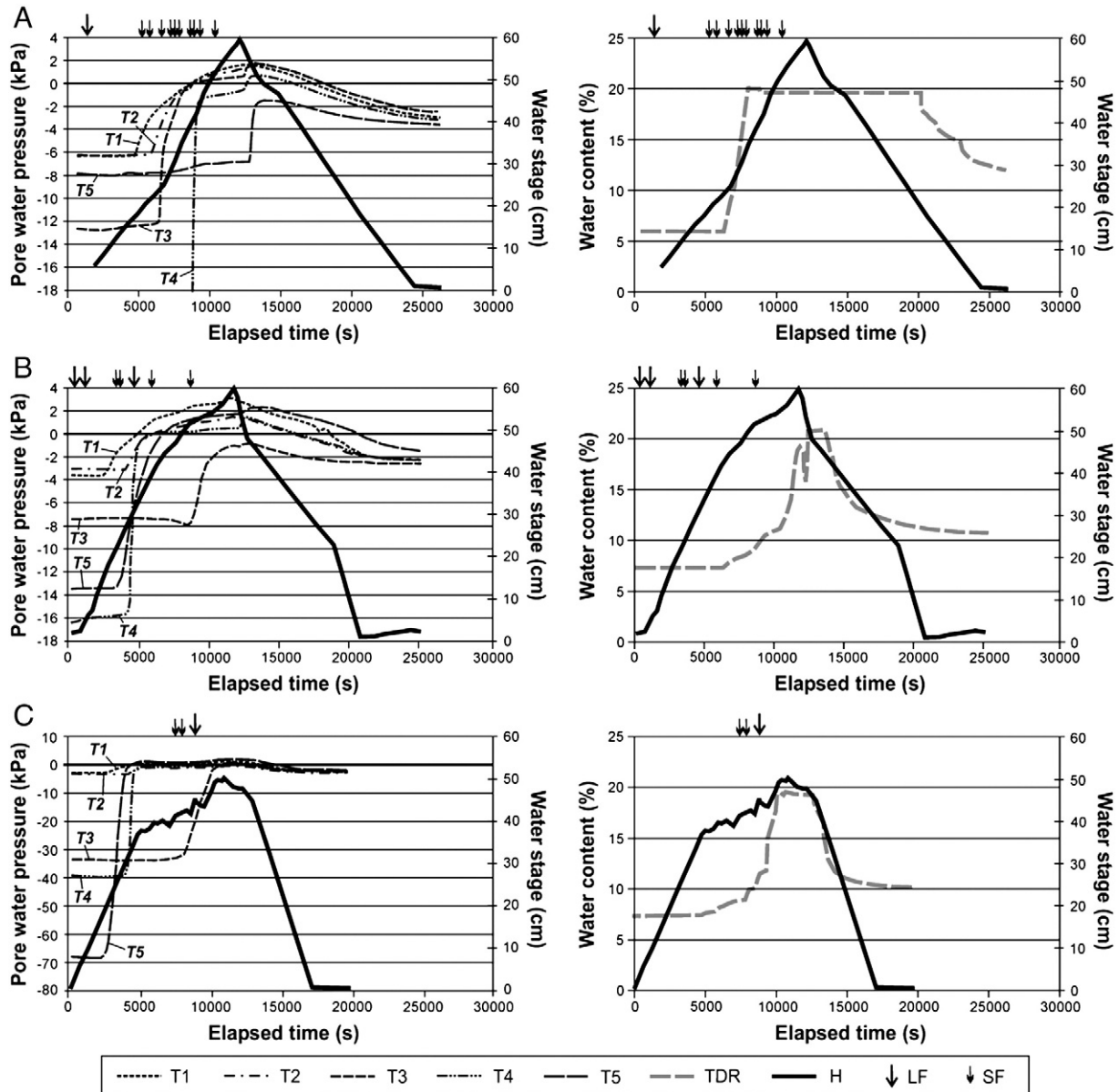
Fig. 7. Trends of measured parameters and summary of failures during EXP1 (A), EXP2 (B), and EXP3 (C): hydrograph, failures, pore water pressures (on the left), and water content (on the right). T1, T2, T3, T4, T5: pore water pressure measured by the tensiometers; TDR: water content measured by the TDR; H: hydrograph; LF: large failures; SF: small failures.

EXP3. For this experiment the same configuration of the sensors as in EXP2 was used. As well as the previous tests, the initial values recorded by the tensiometers are very different (Fig. 7C): T5 measured the lowest value, followed respectively by T4 and T3. This could result from the proximity of these three tensiometers to the porous plate of the lysimeter which dries the material around it. As the water stage increased, between 28.5 and 35 cm, all the tensiometers except T3 started to react. Because of its highest position, T3 started to measure increasing values of pore water pressure when water stage was 41.8 cm, but did not reach saturation. During this experiment, the peak of the hydrograph could not exceed 50.3 cm. The TDR measured water content of the saturated material equal to 19.6% when the water stage was 49.9 cm.

Fig. 7C shows that the increase of the water stage from 36.7 until the peak of the flow was very slow and not constant. This depended on the unexpected high value of conductivity of the bank material. When the water stage exceeded 36.7 cm, the inflow discharge was likely the same as the outflow discharge from the valve at the lysimeter. For that reason, further increase in the water stage was slower and the peak stage was lower than the previous experiments.

The higher conductivity could be explained by the presence of the cement. A hypothesis needing further investigation for future research is that the cement, although in small quantity, was enough to allow for agglomerating the particles, increasing the mean sizes and those of the voids, and therefore, increasing the porosity and the conductivity.

4. Interpretation of results and discussion

A first general consideration is that we observed a large variety of mechanisms of erosion and failures. Previous research has often underestimated the occurrence of mass failures in gravelly bank layers, and this has important implications for modelling bank erosion in composite banks. For example, Rinaldi et al. (2008) and Luppi et al. (2009), in their analysis of a composite riverbank of the Cecina River, excluded mass failures from the basal layer of gravel, because of difficulties in assigning reliable shear strength parameters to such material, and allowed deformation of this layer only by fluvial erosion; this now appears to be a gross simplification. Two aspects are discussed in

the following part of this section: (1) occurrence of erosion and failures because of loss of matric suction; (2) role of factors related to initial instability and to changes in water stage.

4.1. Erosion and failures because of the loss of matric suction

As mentioned previously, erosion because of the loss of matric suction occurred during the rising phase of the hydrograph, with scour forming up to the water surface (in loose sediment), or at a level lower than the water surface (in slightly cemented sediment). This was clearly observed during the initial tests because the initial near-vertical bank face was stable in contact with water, as was the vertical bank-face in EXP3. During EXP1 and EXP2, however, the initial failure immediately after the panel removal caused the failed material to enter into contact with water and cover the basal bank, preventing the direct contact of water with the intact vertical face. Many studies have focussed on seepage erosion, its quantification and triggering conditions. This process is commonly associated to a seepage outflow and implies that a water table gradient is necessary. It occurs during the descending phase of the hydrograph, when the water table can be higher than the river stage. The erosion features observed in our experiments are similar to those classified as seepage-induced erosion and associated to a seepage outflow in many studies (Howard and McLane, 1988; Fox et al., 2006, 2007; Wilson et al., 2007; Lindow et al., 2009). In our study these features, however, have been always observed during the rising phase of the hydrograph, with a gradient from the river into the bank. In case of loose sediment, we associate this process simply to the complete loss of apparent cohesion, because of rapid infilling of the pores within the bank sediment. This causes a disappearance of the weak links among particles, and small-scale breaks and falls occur "particle-by-particle" rather than by mass movements. In this sense, this process can be partly considered as a weakening factor, that is a decrease of the erosion resistance and mechanical stability of the bank material (Thorne et al., 1996), followed by detachment of particles (erosion). When a basal cavity is first created, subsequent falls of small blocks of particle aggregates can also occur. The increasing size of the basal hollow generates a stress-release on the remaining upper portion of the bank, similar to that described for the case of gully head retreat by Collison (2001), inducing the occurrence of cantilever failures.

The same type of process has been also observed in the slightly cemented sediment of EXP3. In this case, the simple loss of apparent cohesion cannot explain the occurrence of erosion, as some effective cohesion exists. The occurrence of erosion was observed to take place at portions of the bank lower than the water stage, that is in submerged conditions. Therefore, this can be explained by the occurrence of positive pore water pressures and an increase in weight of bank sediment, notwithstanding a partial stabilising effect of confining water pressures. The loss of apparent cohesion and the weight of the upper bank material is not balanced by the hydrostatic force. Another possible explanation is that the erosion process was observed to start at the boundary of two basal sub-layers of 10 cm built during the compaction procedure. This created a discontinuity in the bank sediment, favouring water infiltration and, therefore, generating higher local pressures. The enlargement of these fissures was probably the triggering process. Although this process resulted from the construction of the bank, similar discontinuities can be found in nature at the interface of different layers.

These mechanisms observed in our experiments during the rising phases of the hydrograph have rarely been described before, and can represent an important process of basal deformation in gravel layers with low cohesion. Many observations that we have carried out along several composite banks of the Cecina River have revealed the presence of similar features in basal gravel layers, generally attributed to toe fluvial erosion but can also be due to processes similar to those observed in our experiments.

4.2. Initial instability vs changes in pore water pressures

Considering all the observed processes and mechanisms of failure during the experiments, two groups of causes can be considered in creating instability conditions: (1) possible initial instability because of the bank geometry and low shear strength values of the material; and (2) changes in pore water pressure conditions related to changing water stage in the tank.

The first two experiments (EXP1 and EXP2) showed that the failures were possibly related to unstable geometric conditions (excessive bank height and slope for such type of material), because the same material appeared stable for near-vertical slopes with smaller bank heights during the initial tests. This suggests that bank height and slope can play a significant role, and that some critical geometric condition may exist which is difficult to predict a priori because of uncertainties in shear strength parameters and unknown apparent cohesion.

To allow for a better interpretation of the results and to discuss the reciprocal role and relative importance of geometric factors and pore water pressure conditions, some geotechnical analysis was performed. Specific bank stability analyses for observed failures were not possible because of a number of factors, including the difficulty in clearly identifying the failure surface, the absence of specific models for some of the observed mechanisms, and the uncertainty in the shear strength parameters. Therefore, we preferred to use a more general approach based on the construction of stability charts, where the overall stability of the bank is analysed rather than the stability associated with specific mechanisms. This type of approach can be applied to predict the likelihood of bank failure for each of the experiments, after defining its initial geometric conditions (slope and height) and shear strength properties.

In detail, a series of stability charts (bank height versus slope) were created for each experiment (Fig. 8), following the approach used in Rinaldi and Casagli (1999). This entails plotting curves obtained from geotechnical limit equilibrium analysis by using the slope stability charts proposed by Hoek and Bray (1981) for circular failures with a tension crack at a critical depth. This mechanism is considered here as representative of the overall bank instability, rather than associated to specific observed failures (although in two experiments, failures with a component of sliding along a rotational surface were actually observed).

The shear strength of the bank material was quantified according to the failure criterion for unsaturated soils of Fredlund et al. (1978), expressed as follows:

$$\tau = c' + (\sigma - u_a)\tan\phi' + (u_a - u_w)\tan\phi^b \tag{1}$$

where τ = shear strength (kPa), c' = effective cohesion (kPa), σ = normal stress (kPa), u_a = pore air pressure (kPa), ϕ' = effective friction angle (°), u_w = pore water pressure (kPa) and ϕ^b = angle (°) expressing the rate of increase in strength relative to the matric suction ($u_a - u_w$). The previous equation can be also written as:

$$\tau = c + (\sigma - u_a)\tan\phi' \tag{2}$$

where c is the total cohesion, which results from the sum of the effective cohesion c' and the apparent cohesion $c_a = (u_a - u_w)\tan\phi^b$ because of the effects of matric suction (following Dapporto et al., 2003; Darby et al., 2007; Rinaldi and Darby, 2008).

To apply the slope stability charts of Hoek and Bray (1981), dry conditions were considered, and incorporated the negative pore water pressure effects into the total cohesion c.

Determination of shear strength parameters in coarse granular sediment is extremely complex, and it was not possible to directly measure them in this research. Therefore, a series of hypotheses were necessary to define the parameters involved in the analysis, as follows.
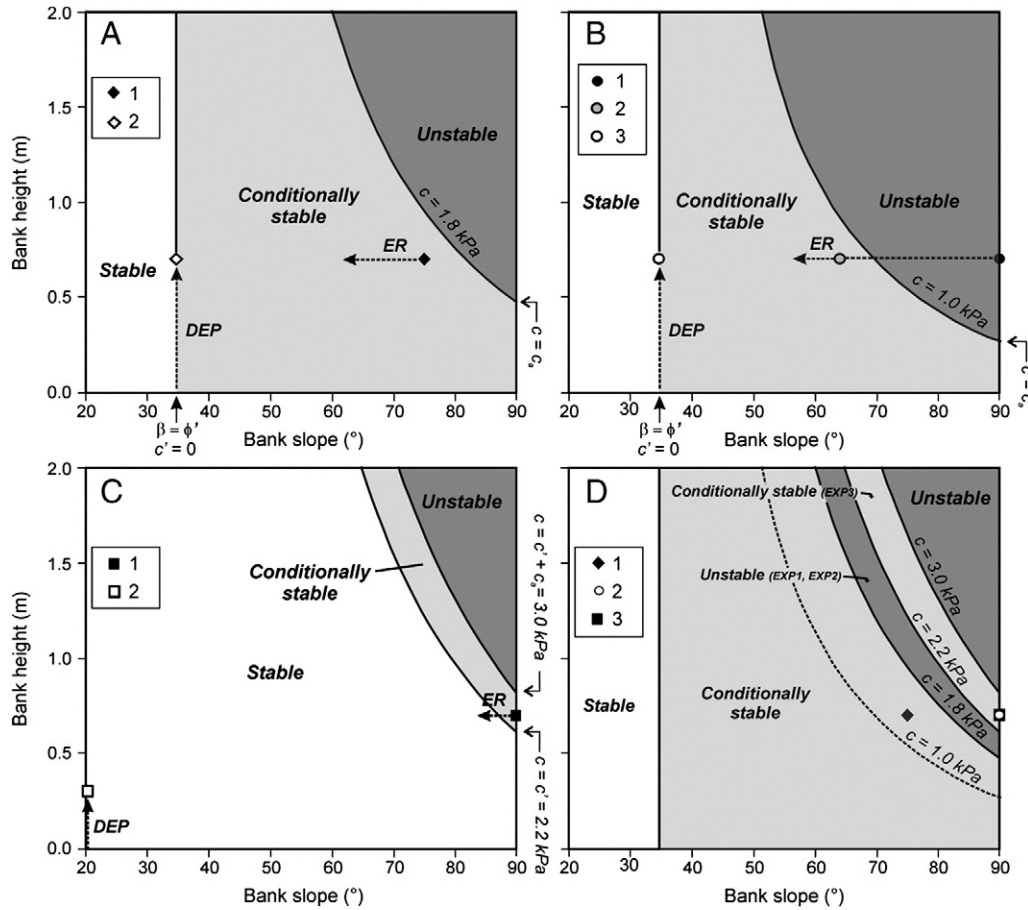
Fig. 8. Stability charts. A: EXP1. 1: Initial bank geometry (packed bank); 2: final bank geometry (loose bank). B: EXP2. 1: Initial bank geometry (packed bank); 2: new bank geometry (after initial failure); 3: final bank geometry (loose bank). C: EXP3. 1: Initial bank geometry (slightly cemented bank); 2: final bank geometry (loose bank). D: summary of all experiments. 1: initial bank geometry of EXP1; 2: initial bank geometry of EXP2; 3: initial bank geometry of EXP3. ER: trajectory of eroding (packed) bank; DEP: trajectory of depositing (loose) basal bank.

(1) For the first two experiments (loose sediment), $c' = 0$, $\phi' = 35°$ were assumed (corresponding to about the observed angle of repose of the sediment), and $\phi^b = 15°$, which is similar to values assumed for low pore water pressures in previous riverbank stability analyses (i.e. Rinaldi et al., 2008).

(2) The pore water pressure measured at the tensiometer T1 (the closest to the bank face) was assumed as the mean value along the whole bank (as a matric suction profile was not available). Based on this value, the initial apparent cohesion was evaluated.

(3) The unit weight γ (kN/m^3) of bank sediment was calculated as:

$$\gamma = \gamma_d + \rho g \theta \qquad (3)$$

where $\gamma_d = 15.2$ kN/m^3 is the unit weight of sediment under completely dry conditions, and θ is the volumetric water content (m^3/m^3), the latter being estimated from the measured initial value at TDR.

(4) Regarding the third experiment (EXP3), an indirect estimation of the effective cohesion c' of the sediment with cement was made, based on the observed geometry of a stable cantilever block (before failure) and assuming the factor of safety equal to 1 (limit equilibrium), by the following equation:

$$FS = \frac{Lc}{\gamma A} \qquad (4)$$

where L is the vertical length (m), c is the mean total cohesion (kPa) given by the sum of effective and apparent cohesion, γ is

the mean unit weight (kN/m^3), and A is the cross-sectional area of the cantilever block (m^2). This analysis provided a value of $c' = 2.2$ kPa. Because the estimation of c' depends on the value of apparent cohesion, the uncertainty was investigated related to the variability of the angle ϕ^b and the pore water pressures. This analysis showed that c' could vary in the range $1.81 \div 2.36$ kPa, with ϕ^b ranging from 35° to 5°, respectively, and in the range $1.84 \div 2.42$ kPa, with $u_a - u_w$ varying from the maximum to the minimum value measured at the closest tensiometers during the experiment. This uncertainty can be considered acceptable, because it did not significantly affect the overall results of the following analysis.

For each experiment an upper curve associated with limit equilibrium for the initial conditions was obtained by using these parameters (Fig. 8). This curve represents the upper bound of stability when the total cohesion is maximum (beginning of the experiment).

Then limit equilibrium conditions were estimated in case of a complete loss of apparent cohesion. For EXP1 and EXP2 (Fig. 8A and B), being $c' = 0$, when $c_a = 0$ and assuming that positive pore pressures have not yet developed, the bank stability does not depend on the bank height, but the bank slope coincides with the friction angle. This is represented by a vertical line with abscissa equal to $\phi' = 35°$, that can be identified as a lower bound corresponding to an ultimate stable angle of the sediment mixture when the total cohesion is equal to zero. For EXP3 ($c' > 0$), the condition associated with $c_a = 0$ is represented by a second curve, on the left of the upper bound (Fig. 8C).

In this way, for each experiment the stability chart can be divided in three regions, defined as follows:

(1) Unstable conditions: above and on the right of the upper bound, the bank is always unstable, including at the beginning of the experiment (a higher value of apparent cohesion would be needed to maintain a stable bank);

(2) Conditionally stable conditions: we define here as conditionally stable the range of geometries of banks between the upper and the lower boundary curves that are stable because of the apparent cohesion, but would be destabilised in case of increasing pore water pressures;

(3) Stable conditions: to the left of the lower bound, the bank is stable even in the case of zero apparent cohesion, and could be destabilised only in case of development of positive pore water pressures.

Although uncertainty occurs in the shear strength parameters, the stability charts allow for a better interpretation of the results for each experiment and for comparing the three experiments (Fig. 8D). A general conceptual sketch of the evolution of bank profiles, interpreted by using this concept, is reported in Fig. 9.

EXP1. The initial bank geometry is in the region of conditionally stable conditions (Fig. 8A), that means that it should remain stable until the apparent cohesion would decrease. Actually, as observed before, the bank is subject to an initial failure. This is not predicted by the stability chart for a series of reasons, including: (1) it is not a rotational failure involving the whole bank, but occurs on the lower portion of the bank; (2) this failure can be associated to the sudden stress release because of removal of the panel, and to the poor compaction of the sediment in that zone from the non-verticality of the bank. The initial failure in turn generates additional stress release on the upper portion and induces a series of cantilever failures. Subsequent failures are associated with increasing pore water pressures (during this phase the upper bound moves towards the left with decreasing apparent cohesion, decreasing the region of conditional stability). The packed eroding bank moves towards the left of the chart (progressively decreasing the slope), whereas a new bank of loose sediment is progressively deposited at a slope approximately equal to the angle of repose.

EXP2. In this case the bank starts from unstable conditions (Fig. 8B). This results from the increase in bank slope and lower initial apparent cohesion. An overall failure immediately occurs after the panel removal. After remodelling the bank, a new failure affects the entire bank, so the profile moves rapidly towards left in the chart (decreasing bank slope), whereas a loose bank is generated at the angle of repose.

EXP3. In this case, it is evident how the presence of a small percentage of cement changes the stability chart, with a much wider region of stable conditions, and a very narrow region of conditionally stable conditions. Nevertheless, the bank is again in the conditionally stable region (Fig. 8C). It has been verified that the bank remains in this region even considering the uncertainty of the effective cohesion, e.g. varying c' in the range $1.81 \div 2.42$ kPa. A change in stability conditions can result from a decrease of apparent cohesion and/or to some modification of the bank geometry by other factors. The bank remains stable until erosion because of the loss of matric suction, occurring with positive pore water pressures (submerged conditions), starts to manifest on the bank toe. At the end, after the occurrence of cantilever failures, the bank geometry of the cohesive portion moves to a slightly lower bank slope, whereas a new wedge of loose material is formed at the bank toe, but with a height significantly lower than the previous experiments.

The bank trajectories shown in the conceptual sketch of Fig. 9 illustrate the occurrence of different dominant processes, starting from different initial bank conditions (I), although some common points can be recognised. The second phase of instability (II) is dominated by slides and granular flows, in case of loose sediment, and by erosion because of loss of matric suction, in case of slightly cemented sediment. The third phase (III) is dominated by the progressive instability of the upper portion by cantilever failures (excluding the unstable banks where cantilevers are unlikely to occur). The final geometry (IV) is distinct in the two cases: (a) in case of loose sediment, the final geometry is the same, independent from the previous bank profile evolution, and corresponds to a plane slope with angle of about the angle of repose of the material; (b) in case of slightly cemented sediment, the final geometry of the intact sediment is almost identical to the initial one (parallel retreat of a near-vertical bank), but with the addition of a wedge of loose sediment with a slope equal to the angle of repose.

To return to the initial geometry, a removal of the sediment accumulated at the base is required (according to the concept of basal endpoint control: Thorne, 1982). In the case of unstable geometry, a temporary increase in shear strength is also required to see such geometry as stable, and this would be possible by an increase in matric suction (i.e. during a relatively dry period) (see for example Rinaldi and Casagli, 1999; Simon et al., 2000; Rinaldi et al., 2004), but these geometries are rare in nature if the sediment has no effective cohesion. Removal of sediment at the bank toe can also occur within a flow (not only during following events): in such a case the result will be to increase the rate of retreat (i.e. Luppi et al., 2009). Actually the cycle of processes can occur more times during runoff, if fluvial erosion removes delivered sediments at the bank toe. In such a case the mass failures would not be limited to the ascending phase of the hydrograph but may also occur during the descending phase. Further investigations would be needed to detail this conceptual model with varying bank characteristics and introducing the removal of basal sediment delivered by bank failures.

These aspects can be crucial in the prediction and interpretation of the planimetric evolution of straight and meandering rivers (see for instance Kobayashi et al., 2008; Dulal et al., 2009).

5. Conclusions

Riverbanks composed of coarse, granular sediment can have a markedly different erosion mechanisms than fine-grained, cohesive banks. Failures in coarse riverbanks tend to occur during the rising phase up to the peak of the hydrograph, mainly as a result of the disappearance of apparent cohesion. Further failures could be possible during the remaining part of the hydrograph. The rate of retreat would increase in case fluvial entrainment removes failed sediment accumulated at the bank toe.

Erosion and failures because of loss of matric suction are significant processes in this type of banks. A basal scour was often observed during the rising phase, and explained as consequence of disappearance of apparent cohesion in loose sediment. In slightly cemented sediment, additional factors can be the development of positive pore water pressures, increase in unit weight of sediment, and the infiltration along the boundary of different layers.

Interpretation of the results by using stability charts clearly show, on a quantitative basis, that the processes of instability observed during the experiments are in most cases the results of a superimposition of factors of initial (geometric) instability, and progressive reduction of apparent cohesion during the experiments. Apparent cohesion is sufficient to maintain a stable bank in loose material, but only for low bank height and/or slopes. Unstable conditions can be triggered when bank material becomes saturated. A very limited percentage of cement is able to explain markedly different responses in terms of stability, mechanisms, and timing of failure. These results may have relevant implications in terms of modelling of bank stability and planimetric evolution of river channels.
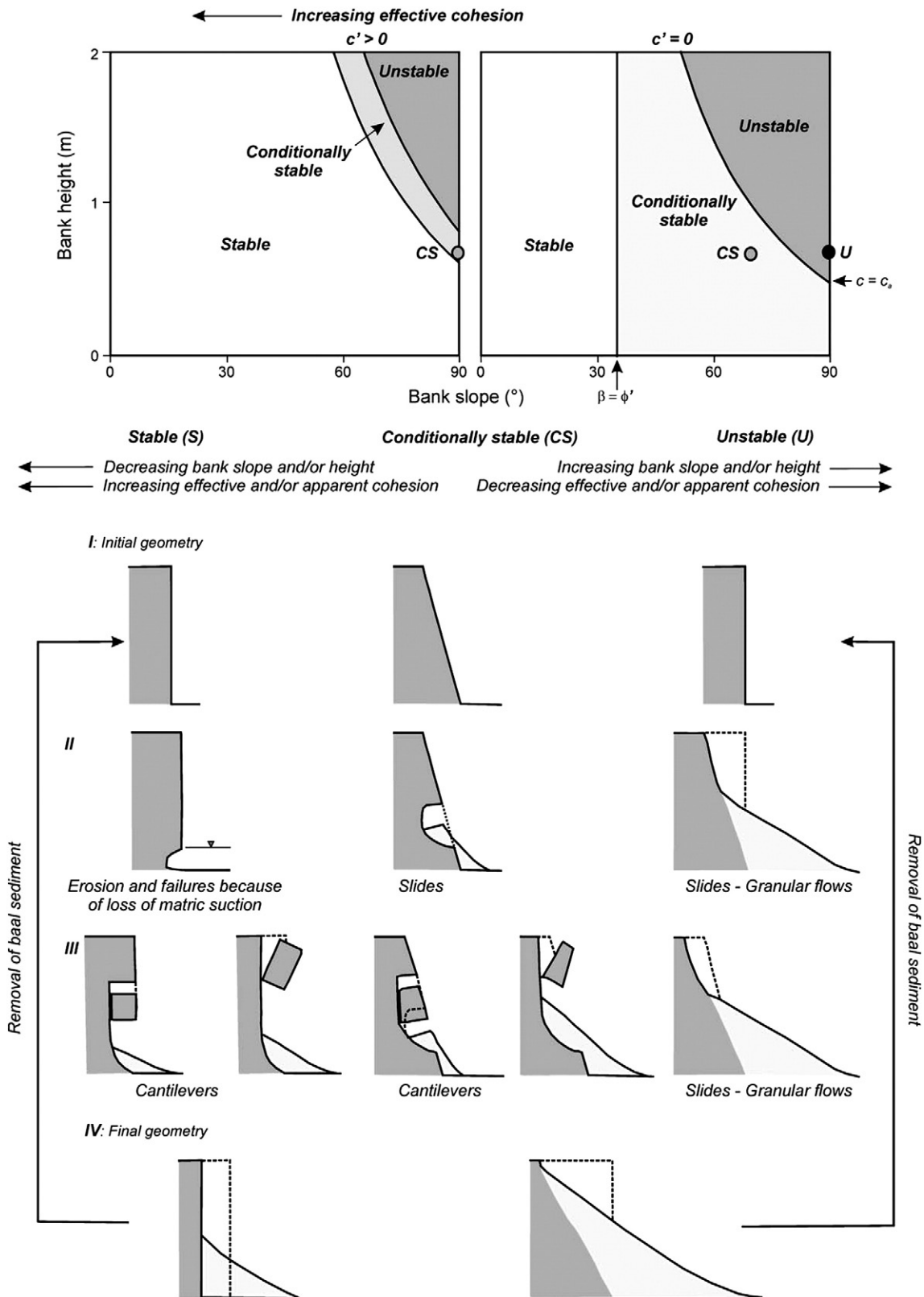
Fig. 9. Conceptual sketch of the evolution of bank profiles, depending on initial conditions.

References

Bradford, J.M., Piest, R.F., 1977. Gully wall stability in loess-derived alluvium. Soil Science Society of America Journal 41, 115–122.

Bradford, J.M., Piest, R.F., 1980. Erosional development of valley-bottom gullies in the Upper Midwestern United States. In: Coates, D.R., Vitak, J.D. (Eds.), Thresholds in Geomorphology, pp. 75–101.

Chen, D., Duan, J.G., 2006. Modeling width adjustment in meandering channels. J. Hydrology 321, 59–76.

Chen, D., Duan, J.G., 2008. Case study: two-dimensional model simulation of channel migration processes in West Jordan River Utah. J. Hydraul. Eng. 134, 315–327.

Collison, A.J.C., 2001. The cycle of instability: stress release and fissure flow as controls on gully head retreat. Hydrol. Process. 15, 3–12.

Dapporto, S., Rinaldi, M., Casagli, N., 2001. Mechanisms of failure and pore water pressure conditions: analysis of a riverbank along the Arno River (Central Italy). Eng. Geol. 61, 221–242.

Dapporto, S., Rinaldi, M., Casagli, N., Vannocci, P., 2003. Mechanisms of riverbank failure along the Arno River, Central Italy. Earth Surface Processes and Landforms 28, 1303–1323.

Darby, S.E., Thorne, C.R., 1996. Development and testing of river-bank stability analysis. J. Hydraul. Eng. 122 (8), 443–454.

Darby, S.E., Rinaldi, M., Dapporto, S., 2007. Coupled simulations of fluvial erosion and mass wasting for cohesive river banks. J. Geophys. Res. 112, F03022. doi:10.1029/2006JF000722.

Dulal, K.P., Kondo, Y., Kimura, I., Shimizu, Y., Parker, G., 2009. Prediction of evolution process in free meandering rivers using 2D numerical model considering slump blocks and inner bank deposition. In: Vionnet, C., García, M.H., Latrubesse, E.M., Perillo, G.M.E. (Eds.), River Coastal and Estuarine Morphodynamics: RCEM 2009, Proceedings RCEM 2009 Symposium, 21–25 September 2009, Santa Fe, Argentina. Taylor & Francis Group, London, pp. 627–634.

Eaton, B.C., 2006. Bank stability analysis for regime models of vegetated gravel bed rivers. Earth Surface Processes and Landforms 31, 1438–1444.

Eaton, B.C., Church, M., Millar, R.G., 2004. Rational regime model of alluvial channel morphology and response. Earth Surface Processes and Landforms 29, 511–529.

Fox, G.A., Wilson, G.V., Periketi, R.K., Cullum, R.F., 2006. Sediment transport model for seepage erosion of stream-bank sediment. J. Hydraul. Eng. 11, 603–611.

Fox, G.A., Wilson, G.V., Simon, A., Langendoen, E.J., Akay, O., Fuchs, J.W., 2007. Measuring streambank erosion due to ground water seepage: correlation to bank pore water pressure, precipitation and stream stage. Earth Surface Processes and Landforms 32, 1558–1573. doi:10.1002/esp. 1490.

Frascati, A., Lanzoni, S., 2009. Morphodynamic regime and long-term evolution of meandering rivers. J. Geophys. Res. 114, F02002. doi:10.1029/2008JF001101.

Fredlund, D.G., Morgenstern, N.R., Widger, R.A., 1978. The shear strength of unsaturated soils. Can. Geotech. J. 15, 312–321.

Haeri, A.M., Hosseini, S.M., Toll, D.G., Yasrebi, S.S., 2005. The behaviour of an artificially cemented sandy gravel. Geotech. Geol. Eng. 23, 507–560. doi:10.2007/s10706-004-5110-7.

Hoek, E., Bray, J.W., 1981. Rock Slope Engineering, Revised 3rd Edition. Istitution of Mining and Metallurgy, London.

Howard, A.D., McLane, C.F., 1988. Erosion of cohesionless sediment by groundwater seepage. Water Resources Research 24, 1659–1674.

Ikeda, S., Parker, G., Sawai, K., 1981. Bend theory of river meanders. Part 1. Linear development. Journal of Fluid Mechanics 112, 363–377.

Kobayashi, K., Dulal, K.P., Shimizu, Y., 2008. Numerical computation of free meandering process of rivers considering the effect of slump block in outer bank region. In:

Altinakar, M.S., Kokpinar, M.A., Aydin, I., Cokgor, S., Kirkgoz, S. (Eds.), River Flow 2008 — Proceedings of the International Conference on Fluvial hydraulics. Turkey, Kubaba Congress Department and Travel Services, pp. 1289–1296.

Lancaster, S.T., Bras, R.L., 2002. A simple model of river meandering and its comparison to natural channels. Hydrol. Process. 16, 1–26. doi:10.1002/hyp. 273.

Lindow, N., Fox, G.A., Evans, R.O., 2009. Seepage erosion in layered stream bank material. Earth Surface Processes and Landforms 34, 1693–1701. doi:10.1002/esp. 1874.

Luppi, L., Rinaldi, M., Teruggi, L.B., Darby, S.E., Nardi, L., 2009. Monitoring and numerical modelling of riverbank erosion processes: a case study along the Cecina River (Central Italy). Earth Surface Processes and Landforms 34, 530–546. doi:10.1002/esp. 1754.

Nagata, N., Hosoda, T., Muramoto, Y., 2000. Numerical analysis of river channel processes with bank erosion. J. Hydraul. Eng. 126, 243–252.

Nardi, L., Rinaldi, M., Solari, L., 2009. Experimental observations on the retreat of non-cohesive river banks. In: Vionnet, C., García, M.H., Latrubesse, E.M., Perillo, G.M.E. (Eds.), River Coastal and Estuarine Morphodynamics: RCEM 2009, Proceedings RCEM 2009 Symposium, 21–25 September 2009, Santa Fe, Argentina. Taylor & Francis Group, London, pp. 89–95.

Rinaldi, M., Casagli, N., 1999. Stability of streambanks formed in partially saturated soils and effects of negative pore water pressures: the Sieve River (Italy). Geomorphology 26, 253–277.

Rinaldi, M., Darby, S.E., 2008. Modelling river-bank-erosion processes and mass failure mechanisms: progress towards fully coupled simulations. In: Habersack, H., Piégay, H., Rinaldi, M. (Eds.), Gravel-Bed Rivers 6 — From Process Understanding to River Restoration. Series Developments in Earth Surface Processes, 11. Elsevier, Netherlands, pp. 213–239.

Rinaldi, M., Casagli, N., Dapporto, S., Gargini, A., 2004. Monitoring and modelling of pore water pressure changes and riverbank stability during flow events. Earth Surface Processes and Landforms 29, 237–254.

Rinaldi, M., Mengoni, B., Luppi, L., Darby, S.E., Mosselman, E., 2008. Numerical simulation of hydrodynamics and bank erosion in a river bend. Water Resources Research 44, W09429. doi:10.1029/2008WR007008.

Seminara, G., 2006. Meanders. Journal of Fluid Mechanics 554, 271–297. doi:10.1017/S0022112006008925.

Simon, A., Curini, A., Darby, S.E., Langendoen, E.J., 2000. Bank and near-bank processes in an incised channel. Geomorphology 35, 193–217.

Soares-Frazao, S., Le Grelle, N., Spinewine, B., Zech, Y., 2007. Dam-break induced morphological changes in a channel with uniform sediments: measurements by a laser-sheet imaging technique. Jour. Of Hydraulic Research 45, 87–95 Extra Issue.

Spinewine, B., Zech, Y., 2007. Small-scale laboratory dam-break waves on movable beds. J. Hydraul. Res. 45, 73–86 Extra Issue.

Spinewine, B., Capart, H., le Grelle, N., Soares Frazão, S., Zech, Y., 2002. Experiments and computations of bankline retreat due to geomorphic dam-break floods. Proceedings of River flow 2002: Louvain-la-Neuve, Belgium, September, 1, pp. 651–661.

Thorne, C.R., 1982. Processes and mechanisms of river bank erosion. In: Hey, R.D., Bathurst, J.C., Thorne, C.R. (Eds.), Gravel-bed Rivers. Wiley, Chichester, pp. 227–271.

Thorne, C.R., Tovey, N.K., 1981. Stability of composite river banks. Earth Surface Processes and Landforms 6, 469–484.

Thorne, C.R., Murphey, J.B., Little, W.C., 1981. Bank stability and bank material properties in the bluffline streams of northwest Mississippi. Appendix D. Report to the U.S. Army Corps of Engineers, Vicksburg District Office, on Stream Channel Stability. 258 pp.

Thorne, C.R., Reed, S., Doorkamp, J.C., 1996. A procedure for assessing river bank erosion problems and solutions. University of Nottingham. National Rivers Authority, R&D Report 28 48 pp.

Wilson, G.V., Periketi, R.K., Fox, G.A., Dabney, S.M., Shields, F.D., Cullum, R.F., 2007. Soil properties controlling seepage erosion contributions to streambank failure. Earth Surface Processes and Landforms 32, 447–459. doi:10.1002/esp. 1405.

Zech, Y., Soares-Frazão, S., Spinewine, B., le Grelle, N., 2008. Dam-break induced sediment movement: experimental approaches and numerical modelling. J. Hydraul. Res. 46, 176–190.